Proc. of the XI Int. Conf. — Ion Implantation and other Applications of Ions and Electrons, Kazimierz Dolny 2016

Two-Dimensional Simulations of H^- Ions Extraction

M. Turek*
Maria Curie Skłodowska University in Lublin, pl. M. Curie-Skłodowskiej 1, 20-031 Lublin, Poland

The 2D particle-in-cell method based model of a negative ion source is presented. The spatial distributions of electrostatic potential and plasma component densities are presented. Changes of negative ion distribution and potential as well as the extracted H^- current with the plasma grid bias voltage are investigated. The presence of the potential well near the plasma grid surface that traps the negative ions is shown. Increase of the H^- ions density inside the chamber with the negative bias voltage is demonstrated. Influence of the H^- ion flux outgoing from the plasma grid on the extracted current was checked: increase by factor 2 is observed when the flux rises 4 times. Current–voltage characteristics of the ion source are presented, saturation of the curve is observed above 50 kV

DOI: 10.12693/APhysPolA.132.254
PACS/topics: 07.77.Ka, 07.05.Tp, 34.35.+a, 41.75.Ak, 41.75.Cn

1. Introduction

Production of intense (order of 100 A/m^2 [1, 2]) negative ion beams is extremely important for future nuclear fusion devices including International Thermonuclear Experimental Reactor (ITER). The neutral beam injection (NBI) systems are considered as efficient (tens of MW per one beamline [3]) plasma heating systems. Radio frequency RF-based negative ion source with multi-aperture extraction grids [4] became a reference device for the ITER project [3].

Detailed knowledge of negative ion production, transport, extraction is necessary in order to design effective ion sources. Computer simulations are useful tools that support that task. A lot of effort has been made in order to model negative ion extraction in both 1D [5], 2D [6] and 3D [7–14]. The results obtained using these codes show e.g. that production of H^- in atom conversion on the caesiated surface leads to H^- ion accumulation near that surface in a potential well. Both 2D and 3D simulations showed also that the extracted negative ion current increases with the magnetic field in the extraction area [15–17] which was also experimentally observed [18]. Detailed studies of H^- and D^- ion production and extraction are in progress using both the trajectory-tracking and self-consistent models [12, 19].

In the paper a 2D model of H^- ion transport and extraction in an initially quasi-neutral plasma is considered. The model is based on the particle-in-cell (PIC) method and is generally very similar to that used in our previous codes [16, 17, 20, 21]. A simplified geometry of the ion source is proposed: a single extraction hole as well as a single flat extraction electrode. It is assumed that H^- ions are produced at the front wall (plasma grid) of the ion source, which is usually covered with a caesium layer [22] in order to lower the work function to ≈ 2 eV (for one monolayer) [23]. The dynamics of H^- ions is not only governed by electric field distribution but also by collisions with other charged particles in the plasma.

The paper contains the brief description of the model and preliminary simulation results as e.g. spatial charge density and potential distributions. Influence of the H^- flux outgoing from the plasma grid surface on the extracted H^- current is under investigation. Changes of the extracted current and plasma potential as well as negative ion distribution due to the negative bias voltage are also examined. Current–voltage characteristics of the ion source are presented and discussed.

2. Simulation model

Simulations were done employing the 2D numerical model of an ionisation chamber and a single flat extraction electrode (positive bias V_{ext}). Negative particles are extracted through a single aperture of 1 mm radius. The schematic view of the system is shown in Fig. 1. The simulation area is covered by a Cartesian 200×100 grid. The cell sizes are $\Delta x = \Delta y = 0.1$ mm. As the electron density of 10^{16} m^{-3} is assumed, this choice fulfills the $\Delta x < 3.4\lambda_D$ criterion where λ_D is the Debye length.

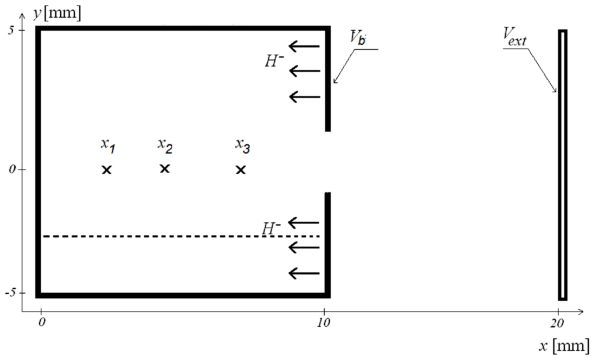

Fig. 1. Schematic view of the simulated system. Dashed line represents $y = -2.5$ mm line (along which the profiles in Figs. 4 and 6 are made).

*e-mail: mturek@kft.umcs.lublin.pl

The model is based on the PIC method [24] assuming that a single pseudo- (or macro-) computational particle represents a large group (of thousands or millions) of particles moving in the same way which reduces the size of a numerical task.

It is assumed that the chamber contains equal numbers of electrons and H^+ ions, each group represented by $3*10^6$ macroparticles. Initially, they are uniformly distributed inside the chamber, with randomly directed velocities, corresponding to the temperature of 1 eV. Charge distribution is calculated using the simplest nearest grid point scheme [25]. The total charge distribution as well as boundary condition determined by electrodes and their voltages are employed to solve the Poisson equation

$$\nabla V(x,y) = \frac{\rho(x,y)}{\varepsilon_0}. \tag{1}$$

This is done using the successive over-relaxation method as in papers [16, 17, 26–30]. Electric field is calculated by numerical derivation of the potential. The classical equations of motion

$$\frac{\mathrm{d}\boldsymbol{v}_i}{\mathrm{d}t} = \frac{q_i}{m_i} E(x,y) \tag{2}$$

are integrated employing the Verlet method [31]. When new positions and velocities of particles are known, the code calculates charge density distribution and steps are repeated until the desired state is achieved.

During simulations the code checks whether a particle hits electrodes. Lost particles are replaced by new ones, randomly placed inside the chamber.

After several thousands of steps some quasi-stationary potential and charge density distribution are achieved and H^- ions are injected into the chamber (N_{H^-} ions per a time step). They are emitted from the inner surface of the front electrode with the velocities corresponding to 0.25 eV. Due to the extraction potential trajectories of some parts of negative ions are deflected towards the extraction electrode. Additionally, the trajectories of H^- ions are randomly modified by e.g. elastic collisions with other particles. This scattering is simulated using the Monte Carlo method based binary collision approximation [32].

The code registers numbers of electrons and ions passing the extraction aperture as well as potential changes in the chosen points inside the chamber. Snapshots of charge density and electrostatic potential distributions may be also saved.

3. Simulation results

Calculations were performed for the extraction voltage $V_{ext} = 2$ kV and 200000 time steps. As the electron velocities inside the chamber and in the extraction aperture do not exceed 10^7 m/s, the choice of $\Delta t = 0.5 \times 10^{-11}$ s fullfils the Courant–Friedrichs–Levy condition [33]:

$$v\Delta t/\Delta x < 1. \tag{3}$$

Evolution of the potential in the points along the ion source axis (marked in Fig. 1) is shown in Fig. 2. After approximately 25000 steps very strong (amplitude of several tens of volts) potential oscillations are damped and a quasi-stationary state is achieved (one should keep in mind that after 30000 steps negative ion starts). One can see that the electrostatic potential has negative values (approximately –8 V to –10 V) along the ion source axis. Due to the screening properties of the plasma, the potential inside the ion source chamber becomes almost flat. One can observe very fast potential oscillations with a frequency of $\approx 5 \times 10^8$ Hz which is comparable to plasma frequency.

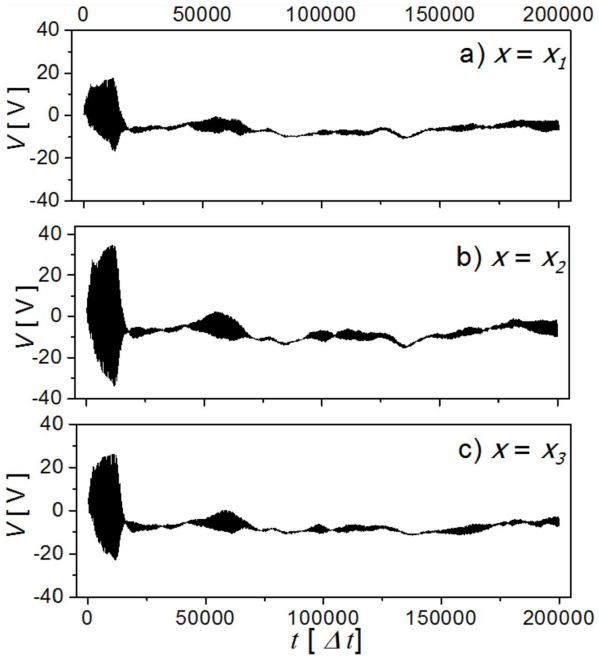

Fig. 2. Potential evolution at the points $x_1 = 2.5$, $x_2 = 5$, and $x_3 = 7.5$ mm.

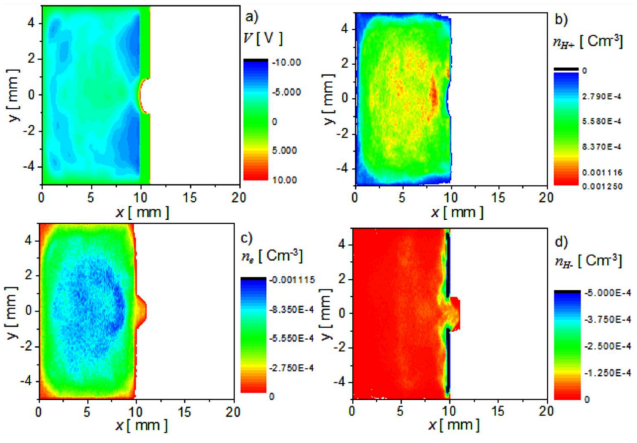

Fig. 3. Potential distribution (a) and charge density distributions for H^+ ions (b), electrons (c) and H^- ions (d). Case of $V_{ext} = 2$ kV and $N_{H^-} = 100$.

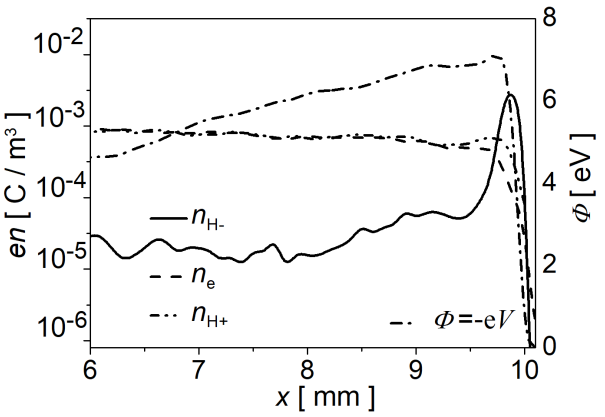

Fig. 4. Profiles along the $y = -2.5$ mm line of charge density distributions as well as the potential energy of H^- ions. The same case as in Fig. 3.

The charge density distributions of electrons, H^+ and H^- ions as well as potential distribution calculated after 200000 time steps for $V_{ext} = 2$ kV and $N_{H^-} = 100$ are presented in Fig. 3. Formation of plasma meniscus in the potential and H^+ charge density distributions can be observed, as the extraction voltage pushes positive ions back inside the ion source chamber. Density of H^- ion is the largest in the middle part of the chamber. Heavier ions are followed by faster electrons that balance their spatial charge, making the potential almost flat in the middle of the chamber. However, a large number of slow H^- ion is emitted form the plasma grid, leading to potential lowering in a 2 mm wide area near the plasma grid. Accumulation of H^- ions near the wall is even better visible in Fig. 4. It shows the plasma components charge density and potential energy profiles (for negative ions) along $y = -2.5$ mm line. One can see that a large number of H^- ions remains very near the plasma grid surface (≈ 0.3 mm thick layer). They are trapped in a ≈ 7 eV deep potential well. The n_e density is lower inside this near-surface well, while positive protons are attracted to it.

Changes of the extracted negative ion current on the H^- current (controlled by the N_{H^-} parameter) outgoing from the plasma grid surface were also under investigation. Figure 5a shows relative changes of the extracted current (normalized to the current obtained for $N_{H^-} = 100$, i.e. $\delta I = (I - I(N_{H^-} = 100))/I(N_{H^-} = 100))$ for N_{H^-} up to 400. One can see that increasing N_{H^-} leads initially to the higher H^- ion yield but for larger N_{H^-} one observes saturation of that trend. This is due to (i) the above mentioned potential well near the surface that traps the negative ions and (ii) low velocity (compared to electrons) of H^- ions.

Influence of the negative bias voltage V_b of the plasma electrode on the extracted current was also examined. The simulation results for V_b equal to 0, –5 V and –10 V are shown in Fig. 5b. The H^- current is increased by only $\approx 6\%$ in the case of $V_b = -10$ V. The yield due

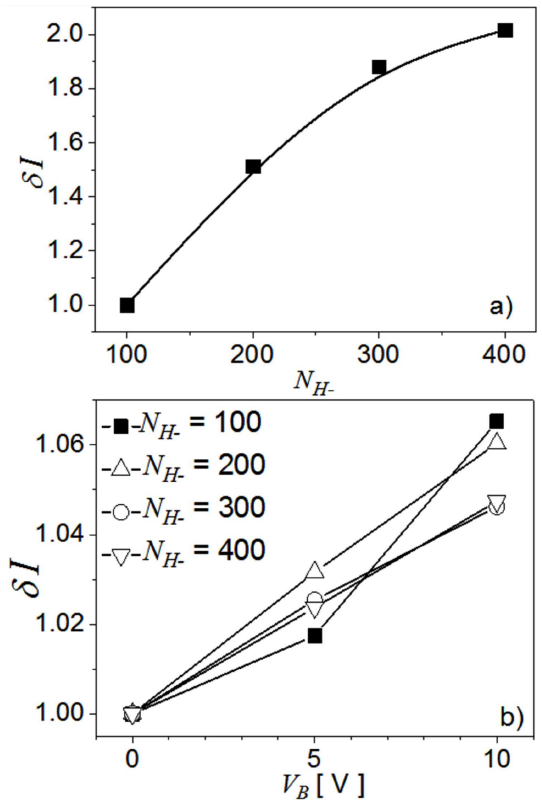

Fig. 5. Relative changes of the extracted H^- current $\delta I = (I - I(N_{H^-} = 100))/I(N_{H^-} = 100)$ due to the surface outgoing H^- flux N_{H^-} (a) and plasma grid bias V_b (b).

to the V_b is smaller for the higher outgoing flux of H^- ions (N_{H^-} equal to 300 or 400). One can see (Fig. 6a) that H- density in a 3 mm wide region near the electrode increases almost by a decade when V_b is set to –10 V. This results in lowering of the electrostatic potential V (and increase of $\Phi = -eV$, shown in Fig. 6b). On the other hand, the depth of the potential well near the surface remains almost unchanged.

The current–voltage characteristics of the ion source for $N_{H^-} = 100$ and $N_{H^-} = 400$ were also calculated. Simulations were done for $V_b = 0$ and V_{ext} up to 70 kV. The dependence of the extracted ion current on the simulation time for $N_{H^-} = 400$ is presented in Fig. 7a. The extracted current is averaged over 60 μs. The average value of the flat part of the curve is assumed as the final value of the H^- current. The current–voltage curves are shown in Fig. 7b. A fast increase of the current is observed up to 20 kV and it is followed by the saturation for V_{ext} higher than 50 kV (the case of $N_{H^-} = 100$). For $N_{H^-} = 400$ the saturation requires higher V_{ext} (above 70 kV).

4. Conclusions

A 2D model of negative ion production, transport and extraction, based on the particle-in-cell method is pre-

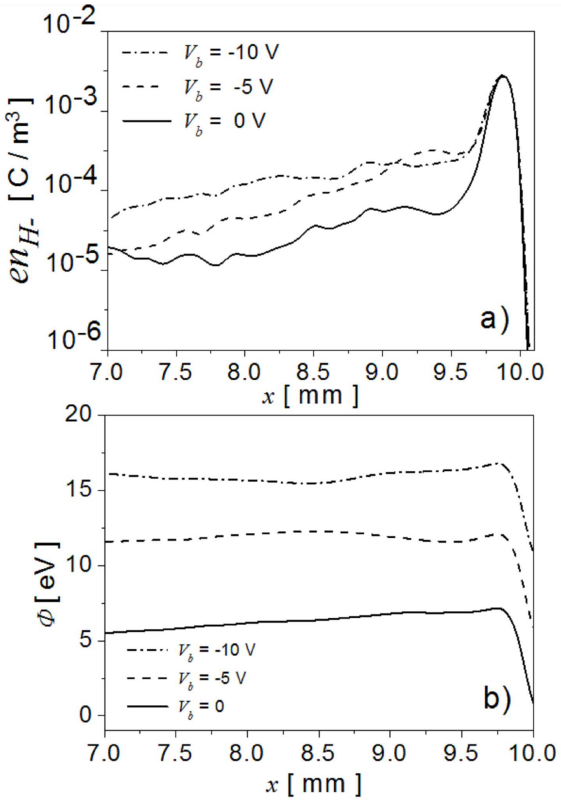

Fig. 6. H^- charge density distributions (a) and their potential energy (b) for different V_b.

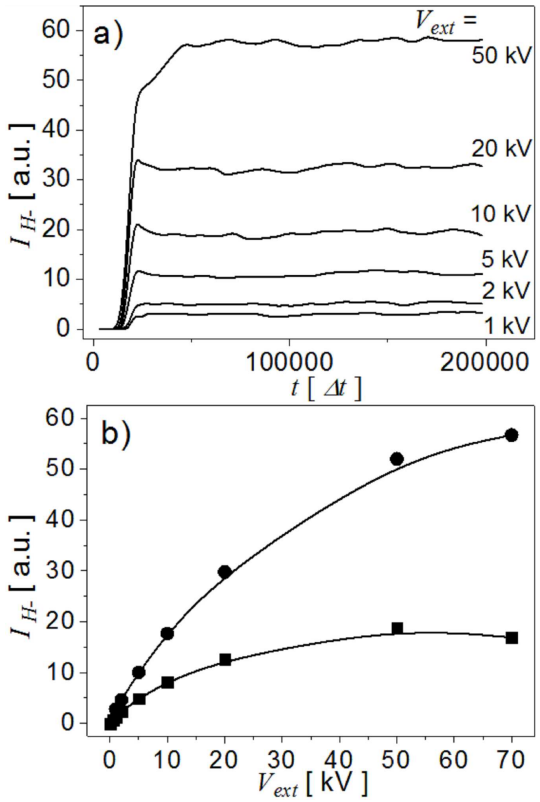

Fig. 7. Extracted H^- currents for different V_{ext} as a function of time (a) and current–voltage curve (b).

sented. The numerical code follows the trajectories of H^- and H^+ ions as well as electrons in a self-consistent manner and provides e.g. charge density and potential distributions, dependences of extracted ion and electron currents etc. Stabilization of the plasma potential after several tens of thousands of iteration is achieved — negative potential (≈ -8 V) is due to the H^- ion injection. Formation of the plasma meniscus near the extraction aperture is observed in the potential and H^+ density distributions. It was found that most of H^- gather in a thin layer near the plasma grid due to formation of potential well, these results are similar to those obtained by other simulations [5, 9]. Increase of the H^- flux outgoing form the plasma grid leads to the rise of extracted H^- current but that trend saturates above a certain level ($N_{H^-} = 100$ in the considered case). The influence of negative bias voltage applied to the plasma grid was also under investigation. Despite the fact that V_b =–10 V increases the density of H^- by an order of magnitude, the increase of H^- current by approximately 6% is most probably due to the fact that the above-mentioned potential well depth does not significantly change. Current–voltage characteristics of the ion source were calculated. The saturation of the I–V curve was found for the voltages above 50 kV ($N_{H^-} = 100$).

References

[1] P. Franzen, L. Schiesko, M. Froschle, D. Wunderlich, U. Fantz, and the NNBI-Team, *Plasma Phys. Control. Fusion* **53**, 115006 (2011).

[2] W. Kraus, U. Fantz, P. Franzen, M. Fröschle, B. Heinemann, R. Riedl, D. Wünderlich, *Rev. Sci. Instrum.* **83**, 02B104 (2012).

[3] R. Hemsworth, A. Tanga, V. Antoni, *Rev. Sci. Instrum.* **79**, 02C109 (2008).

[4] E. Speth, H.D. Falter, P. Franzen, U. Fantz, M. Bandyopadhyay, S. Christ, A. Encheva, M. Fröschle, D. Holtum, B. Heinemann, W. Kraus, A. Lorenz, Ch. Martens, P. McNeely, S. Obermayer, R. Riedl, R. Süss, A. Tanga, R. Wilhelm, D. Wünderlich, *Nucl. Fusion* **46**, 220 (2006).

[5] D. Wunderlich, R. Gutser, U. Fantz, *Plasma Sourc. Sci. Technol.* **18**, 045031 (2009).

[6] J.P. Boeuf, J. Claustre, B. Chaudhury, G. Fubiani, *Phys. Plasmas* **19**, 113510 (2012).

[7] G. Fubiani, J.P. Boeuf, *Plasma Sourc. Sci. Technol.* **24**, 055001 (2015).

[8] K. Kourtzanidis, J.P. Boeuf, F. Rogier, *Phys. Plasmas* **21**, 123513 (2014).

[9] S. Mochalskyy, A.F. Lifschitz, T. Minea, *J. Appl. Phys.* **111**, 113303 (2012).

[10] S. Mochalskyy, A.F. Lifschitz, T. Minea, *Nucl. Fusion* **50**, 105011 (2010).

[11] S. Mochalskyy, D. Wuenderlich, B. Ruf, U. Fantz, P. Franzen, T. Minea, *Plasma Phys. Control. Fusion* **56**, 105001 (2014).

[12] S. Mochalskyy, D. Wuenderlich, U. Fantz, *Nucl. Fusion* **55**, 033011 (2015).

[13] F. Taccogna, P. Minelli, S. Longo, *Plasma Sourc. Sci. Technol.* 22, 045019 (2013).

[14] D. Wünderlich, R. Gutser, U. Fantz, *AIP Conf. Proc.* **925**, 46 (2007); D. Wunderlich, L. Schiesko, P. McNeely, U. Fantz, P. Franzen, and the NNBI-Team, *Plasma Phys. Control. Fusion* **54**, 125002 (2012).

[15] T. Sakurabayashi, A. Hatayama, M. Bacal, *J. Appl. Phys.* **95**, 3937 (2004).

[16] M. Turek, J. Sielanko, P. Franzen, E. Speth, *AIP Conf. Proc.* **812**, 153 (2006).

[17] M. Turek, J. Sielanko, *Vacuum* **83**, 256 (2009).

[18] M. Bacal, J. Bruneteau, P. Devynck, *Rev. Sci. Instrum.* **59**, 2152 (1988).

[19] D. Wunderlich, S. Mochalskyy, U. Fantz, and NNBI-Team, *Plasma Sourc. Sci. Technol.* **23**, 015008 (2014).

[20] M. Turek, K. Pyszniak, A. Droździel, J. Sielanko, A. Latuszyński, D. Mączka, Y.A. Vaganov, Y.V. Yushkevich, *Instrum. Exp. Techn.* **52**, 90 (2009).

[21] A. Pyszniak, A. Droździel, M. Turek, A. Latuszyński, D. Mączka, J. Sielanko, Yu.A. Vaganov, Y.V. Yushkevich, *Instrum. Exp. Techn.* **50**, 552 (2007).

[22] U. Fantz, P. Franzen, W. Kraus, M. Berger, S. Christ-Koch, M. Fröschle, R. Gutser, B. Heinemann, C. Martens, P. McNeely, R. Riedl, E. Speth, D. Wünderlich, *Plasma Phys. Control. Fusion* **49**, B563 (2007).

[23] W.G. Graham, in: *Proc. 2nd Int. Symp. Production Neutralisation Negative Hydrogen Ions Beams, New York*, Ed. Th.J.M. Sluyters, Brookhaven National Laboratory, Upton (NY) 1980, p. 126.

[24] C.K. Birdsall, A.B. Langdon, *Plasma Physics Via Computer Simulation*, McGraw-Hill, New York 1985.

[25] M. Brzuszek, M. Turek, J. Sielanko, *Ann. UMCS. Informat. AI* **5**, 201 (2006).

[26] M. Turek, A. Drozdziel, K. Pyszniak, S. Prucnal, J. Żuk, *Przegląd Elektrotechniczny* **86**, 193 (2010), (in Polish).

[27] M. Turek, K. Pyszniak, A. Drozdziel, J. Sielanko, *Vacuum* **82**, 1103 (2008).

[28] M. Turek, K. Pyszniak, A. Droździel, *Vacuum* **83**, S260 (2009).

[29] M. Turek, *Acta Phys. Pol. A* **123**, 847 (2013).

[30] M. Turek, *Acta Phys. Pol. A* **120**, 188 (2011).

[31] W.C. Swope, H.C. Andersen, P.H. Berens, K.R. Wilson, *J. Chem. Phys.* **76**, 637 (1982).

[32] S. Ma, R.D. Sydora, J.M. Dawson, *Comput. Phys. Commun.* **77**, 190 (1993).

[33] R. Courant, K.O. Friedrichs, H. Levy, *Math. Ann.* **100**, 32 (1928).